Sensors & Transducers, Vol. 216, Issue 9-10, September-October 2017, pp. 29-37

www.sensorsportal.com

Sensors & Transducers

Published by IFSA Publishing, S. L., 2017
http://www.sensorsportal.com

Molecular Doping on Epitaxial Graphene by Gaseous Surface Adsorbents: Influence of Interband Scattering

B. K. Daas, Goutam Koley and T. S. Sudarshan
Department of Electrical and Computer Engineering, University of South Carolina
301 S. Main St, Columbia, SC 29208, USA
E-mail: Daas@email.sc.edu

Received: 9 August 2017 /Accepted: 17 October 2017 /Published: 31 October 2017

Abstract: We investigate molecular adsorption doping by electron withdrawing NO_2 and electron donating NH_3 on epitaxial graphene grown on C-face 6H-SiC substrates. We reconcile models describing the conductivity of graphene at low and high frequencies in the relaxation time approximation. These equations are applied to develop theoretical model for adsorption of NO_2 and NH_3 molecules on an epitaxial graphene surface probed by infrared reflectance, a non-destructive technique for transport studies in graphene. We separate the intraband and interband scattering contributions to the electronic transport under gas adsorption. We find that only by including a significant interband (intraband) contribution can measured reflectance be fit accurately at low (high) frequency regime. Interband relaxation times as short as ~0.1 fs are obtained under gas adsorption, much shorter than previously assumed (~100 fs), leading to a breaking of the usual universal conductivity observed in purer samples. This method can also calculate percentage charge transfer by NO_2 to graphene (1~2 %) and NH_3 to graphene (0.01~0.1 %). Finally, this transport behavior indicate that, under gas adsorption, the influence of interband scattering cannot be neglected, even at DC

Keywords: Graphene, Molecular adsorption doping, Interband Scattering, Gas adsorption

1. Introduction

Graphene is a revolutionary zero bandgap nanomaterial that demonstrates remarkable properties, such as high electron mobility [1], the highest Young's modulus ~1 TPa [2], the highest thermal conductivity of any known material [3] and single molecule sensitivity to gases [4]. This unique electronic properties arises from it's massless Dirac-like linear dispersion ($E = hkv_F$) of electrons [1], where E is the energy, h is the plank's constant, k is the Fermi wave vector and v_F is the Fermi velocity (Fig. 1(a). This linear dispersion relation is in contrast to the traditional quadratic dispersion commonly exhibited by most semiconductors; introduce a new class of electronic material for sensing and device application. This truly 2D structure can be doped to high value of electron and hole concentration either by applying external voltage, much like an FET or with the molecular and adsorption doping. Molecular doping on both exfoliated and epitaxial graphene has been successfully studied. The charge impurity of exfoliated graphene was studied by J. H. Chen, *et al.*, [5] where graphene was doped by potassium and Tetra-cyanoquino-di-methane (TCNQ) at ultra high vacuum. Potassium doping on epitaxial graphene has also been studied by A. Bostwick, *et al.* [6], where growth, EG/SiC interface and electronic property has been discussed. These kinds of control over electrical properties of material are the heart of modern electronics such as FET and sensors.

The good sensor properties of carbon nanotubes are already known for some time, [7] but recently, the

possibility to use graphene as a highly sensitive gas sensor was also reported [4]. Graphene on SiC substrate (EG) offers the added advantage of integrating sensors and readout circuits on the same chip, that are also suitable for harsh environment operation, taking advantage of the wide band gap of SiC [8]. It was shown that the increase in graphene charge carrier concentration induced by adsorbed gas molecules can be used to make highly sensitive sensors, even with the possibility of detecting individual molecules. These excellent sensor properties of graphene are due to two important facts:

1) Graphene is a two-dimensional crystal with only a surface and no volume, which maximizes the effect of surface dopants;

2) Graphene is highly conductive and shows metallic conductance even in the limit of zero carrier density.

These sensor properties are based on changes in the resistivity due to molecules adsorbed on the graphene sheet that act as donors or acceptors. It is well established that EG surface conductivity can be varied by molecular adsorption doping where conductivity is a tradeoff between carrier concentration and scattering [9].

The sensitivity of exfoliated graphene to NH_3 and NO_2 [10] and that of epitaxial graphene (EG) [11] have been established by molecular adsorption doping where the adsorbent NH_3 and NO_2 acts as electron donating and withdrawing characteristics respectively. Thus EG surface electron concentration can either increase or decrease depending on whether the adsorbent is electron donating or withdrawing. These adsorbents can also influence carrier scattering, all of which change the surface conductivity. In our earlier paper [12] we established a change of conductivity due to molecular adsorption doping by amperometric (DC) measurements. In this paper we emphasize carrier transport studies through Fourier transform infrared (FTIR) measurement for molecular adsorption doping within the frequency range of 10 THz to 100 THz. Theoretically, we account for the influence of surface impurities on the conductivity of EG by molecular gas adsorption [10] using the Boltzmann picture, consistent with our experiment. Thus the reconciliation of EG conductivity of low and high frequency is important to investigate the transport properties in mid IR regime.

2. Theory

2.1. Derivation of EG Conductivity

A detailed model of the electrical and optical conductivity from direct current (DC) to the infrared is required to enable this investigation. In any material, the conductivity can be divided into two components, intraband and interband conductivities. Intraband conductivity refers to the traditional Drude-Sommerfeld type conductivity involving free electrons (holes) in the conduction (valence) band. Scattering events here only move carriers within the same band named intraband scattering. Interband conductivity accounts for processes where carriers can move between bands, such as direct optical absorption and carrier recombination. Scattering events here lead to carriers changing bands known as interband scattering. Fig. 1(a) illustrates these two conduction modes in EG where Fermi level position is also indicated.

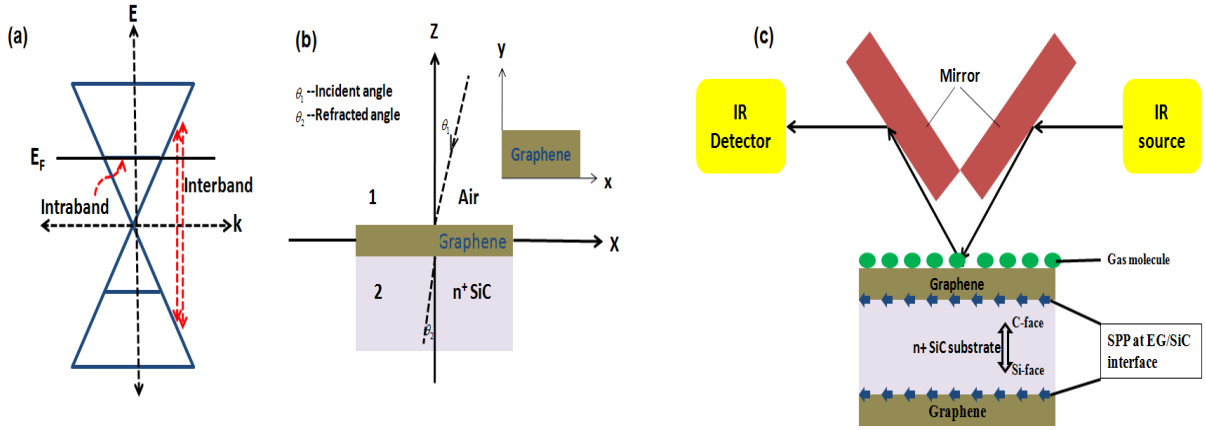

Fig. 1. (a) Plot of EG linear dispersion relation ($E = hkv_F$), Fermi level E_F is shown and intra and interband transition regime is indicated; (b) Shows reflection from EG where graphene is considered between air and SiC interface; (c) Experimental set-up for IR reflection spectroscopy for molecular adsorption measurement.

Gusynin, *et al.*, [13] adopt a Kubo-Green formalism to describe the interband and intraband conductivity of graphene. While this is a complete and rigorous description, it is somewhat complex, and hides the "Boltzmann-like" diffusive transport inherent in it. Furthermore, in the original formulation [14], the relaxation times used for the interband and intraband terms are identical. While this is a good

starting point, the measurements presented later in the paper show that this is not accurate. In fact, there is no a priori reason why the relaxation times for the two very different conduction modes should be the same. Introducing separate scattering times τ_{intra} and τ_{inter} for intraband and interband conduction modes respectively, these equations for the optical conductivity can be written as [13];

$$\sigma_{intra} = \frac{e^2}{\pi\hbar}\frac{i}{\omega + i/\tau_{intra}}\int_{-\infty}^{+\infty} d\varepsilon(-\frac{\delta f(\varepsilon-\varepsilon_f)}{\delta\varepsilon})\varepsilon^2\frac{\theta(\varepsilon^2)}{|\varepsilon|}, \quad (1)$$

$$\sigma_{inter} = i\frac{e^2(\omega + i/\tau_{inter})}{\pi}\int_0^{+\infty}\frac{d\varepsilon[f(\varepsilon-\varepsilon_f)-f(-\varepsilon-\varepsilon_f)]}{(2\varepsilon)^2-\hbar^2(\omega+i/\tau_{inter})^2}, \quad (2)$$

where e is the electronic charge, ε is the energy variable over which integration takes place, ε_f is the Fermi level, ω is the frequency of the incident electromagnetic radiation, $f(\varepsilon) = [\exp(\varepsilon/kT)+1]^{-1}$ is the Fermi-Dirac distribution function, k is the Boltzman constant $1.3806503 \times 10^{-23}$ m^2 kg $s^{-2}K^{-1}$ and θ is the Heaviside step function. We note that throughout this paper, SI units are used, unless otherwise indicated.

2.2. Intraband Conductivity

The DC intraband conductivity can be understood in the Boltzmann transport picture from Equation (1). By assuming that the temperature is low i.e. $\varepsilon_f >> kT$, the Fermi functions, f, in Equation (1) can be replaced by step functions, leading to the approximation,

$$\int_{-\infty}^{+\infty} d\varepsilon(-\frac{\delta f(\varepsilon-\varepsilon_f)}{\delta\varepsilon})\varepsilon^2\frac{\theta(\varepsilon^2)}{|\varepsilon|} = \varepsilon_f \quad (3)$$

Putting this value in eq-1 and considering $\omega = 0$ we get the DC conductivity as follows

$$\sigma_{intra} = \frac{e^2\tau_{intra}\varepsilon_f}{\pi\hbar} \quad (4)$$

Carrier concentration is given by…

$$n = \int_0^{\infty} D(\varepsilon) f(\varepsilon-\varepsilon_F) dE \quad (5)$$

where D(ε) is the density of states in graphene. $D(\varepsilon) = 2\varepsilon/\pi(\hbar v_F)^2 \approx 1.46\times10^{14}$ E cm^{-2}.

Replacing this value in Equation (4) and using Fermi Dirac distribution $E = hkv_F$), we get...

$$\sigma_{intra} = ne^2v_f^2\tau_{intra}/\varepsilon_f = ne^2\tau_{intra}/m_{rel} = ne\mu, \quad (6)$$

where we have used the relativistic relation $\varepsilon_f = m_{rel}v_f^2$ in the last step for the relativistic mass-like term m_{rel}. Thus, the Kubo formula can be thought of as a relaxation time modification to the Boltzmann conductivity and shows the equivalence of the 2 pictures.

2.3. Interband Conductivity

We begin by assuming that there is negligible broadening of the interband transitions i.e. long τ_{inter}. With this assumption, and by taking low temperatures, giving $\varepsilon_f >> kT$, we can replace the Fermi functions in Equation (2) above with step functions.

$$\begin{aligned}\sigma_{inter} &= \frac{ie^2\omega}{4\pi}\int_0^{\infty}\frac{d\varepsilon[f(\varepsilon-\varepsilon_f)-f(-\varepsilon-\varepsilon_f)]}{(\varepsilon)^2-(\hbar\omega/2)^2} \\ &= \frac{ie^2\omega}{4\pi}\int_{\varepsilon_f}^{\infty}\frac{d\varepsilon}{(\varepsilon)^2-(\hbar\omega/2)^2} \\ &= \frac{ie^2\omega}{4\pi}\frac{1}{\hbar\omega}\ln(\frac{\varepsilon_f-\hbar\omega/2}{\varepsilon_f-\hbar\omega/2}\end{aligned}, \quad (7)$$

where we have used partial fractions to evaluate the final step. The frequency term ω, in the coefficient cancels out, leaving the logarithmic term. In the limit $\omega\to\infty$, $\sigma_{inter}\to e^2/4\hbar$, independent of frequency, the so-called universal conductivity of graphene [15].

Now, we reintroduce the interband broadening through the relaxation time approximation. This is done by replacing $\omega \longrightarrow \omega + i/\tau_{inter}$. Now, again in the limit $\omega\to\infty$, we recover the universal conductivity. However, when $\omega << \tau_{inter}^{-1}$, the conductivity can deviate significantly from the universal conductivity. In fact, for $\tau_{inter} = 5fs$, a reasonable value in some situations (more data below), the conductivity can deviate significantly from the universal value even in the infrared and visible regimes.

We thus consider the low frequency regime i.e. $\omega \longrightarrow 0$. In this limit,

$$\sigma_{inter} = \frac{ie^2}{4\pi\hbar}\ln(\frac{\varepsilon_f - i\hbar/2\tau_{inter}}{\varepsilon_f + i\hbar/2\tau_{inter}}) = \frac{ie^2}{4\pi\hbar}\ln(e^{-2iX}) = \frac{e^2X}{2\pi\hbar}, \quad (8)$$

where $X = \arctan(\hbar/2\varepsilon_f\tau_{inter})$. We now make the assumption that $X << 1$ i.e., ε_f is large >> kT i.e. low temperature and/or τ_{inter} is long. This is a reasonable assumption, for typical values of ε_f ~0.2 eV and τ_{inter} as short as 5fs. This allows us to approximate $X = \arctan(\hbar/2\varepsilon_f\tau_{inter}) \approx \hbar/2\varepsilon_f\tau_{inter}$. Thus, Equation (8) becomes

$$\sigma_{\text{inter}} = \frac{e^2}{4\pi\varepsilon_f \tau_{\text{inter}}}, \quad (9)$$

which is identical to the result obtained by Liu, *et al.*, [16] using a kinetic approach for DC. Thus, the equivalence of the full optical model and the DC kinetic model for the interband conductivity is demonstrated. A key conclusion of Equation (9) is that even at DC i.e., $\omega = 0$, *there is a non-negligible interband contribution* to the conductivity of graphene. We will later present experimental evidence for this behavior.

2.4. Reflection

Considering graphene at the interface between two dielectrics (shown in Fig. 1(b) with dielectric functions ε_1 and ε_2, the total reflectivity is given by [17]

$$R = \frac{\left| \left(\sqrt{\varepsilon_1 \varepsilon_2(\omega)\varepsilon_0} / \alpha \right) + \frac{\sqrt{\varepsilon_1} N\sigma(\omega) \times \cos(\Phi 1)}{c} - \varepsilon_1 \varepsilon_0 \right|^2}{\left| \left(\sqrt{\varepsilon_1 \varepsilon_2(\omega)\varepsilon_0} / \alpha \right) + \frac{\sqrt{\varepsilon_1} N\sigma(\omega) \times \cos(\Phi 1)}{c} + \varepsilon_1 \varepsilon_0 \right|^2} \quad (10)$$

where $\alpha = \frac{\sqrt{1-[(\frac{n_1}{n_2}\sin\Phi 1)]^2}}{\cos\Phi 1}$ n_1 and n_2 are the refractive index of air and SiC respectively, σ(ω) is the total conductivity, ε_0 is the free space permittivity (~8.854×10^{-12} F/m). For EG on SiC substrates, ε_1 is the permittivity of air (~1) and ε_2 is the permittivity of SiC, which is a function of wavelength, given by [18]

$$\varepsilon_2(\omega) = \varepsilon_\infty \frac{\omega^2 - \omega_{LO}^2 + i\Gamma_1\omega}{\omega^2 + \omega_{TO}^2 + i\Gamma_2\omega}, \quad (11)$$

where ε_∞ =6.5 is the positive ion core background dielectric constant, ω_{LO} is the longitudinal optical phonon frequency (ω_{LO} =972cm^{-1}), ω_{TO} is the transverse optical phonon frequency (ω_{TO} =796 cm^{-1}). $\Gamma_{1,2}$ describes the broadening of the phonon resonances, typically 5-60 cm^{-1}, where the higher values are due to free-carrier absorption.

Within this theoretical framework, we investigate the carrier transport by FTIR reflection spectroscopy, while theory matches with experimental results to extract various transport parameters, including the influence of interband scattering, which is non-negligible at IR frequencies and high surface impurity concentrations. Finally we show the role of interband scattering on impurity concentration.

3. Experimental

Epitaxial growth of large-area graphene by thermal decomposition of commercial <0001> 4H and 6H SiC substrates at high temperature and vacuum has been demonstrated [19]. This produces EG a few monolayer, ML to >50 ML thick, depending on growth conditions. In our experiments, EG was grown on commercial n^+ 8^0 off axis 4H-SiC substrates on C-face, nitrogen doped ~10^{19}/cm^3. 1 cm×1 cm samples were degreased using trichloroethylene, acetone and methanol respectively. They were then rinsed in DI water for three minutes. The samples were finally dipped in HF for two minutes to remove native oxide and rinsed with DI water before being blown dry. They were then set in the crucible in an inductively heated furnace where high vacuum was maintained (<10^{-6} Torr) and baked out at 1000 ^{0}C for 13 to 15 hours. The temperature was slowly raised to the growth temperature (1250-1400^{0}C). All growths were performed for 60 minutes before cooling to 1000 ^{0}C at a ramp rate of 7~8^{0}C/min and eventually to room temperature. Slow temperature ramps were utilized to minimize thermal stress on the samples.

For this study, our focus is on epitaxial graphene on C-face because defects have been attributed to the EG grown on C-face SiC [20]. Fourier Transform Infrared reflection (FTIR) spectra gives the differential reflectance with respect to a reference. For EG reflection spectra, SiC substrate used as a reference for the respective gas medium. Defects on EG layer (grown on C-face SiC) allow diffusion of gas through the defects point justifies the similar reference maintain under particular gaseous medium.

After growth AFM (atomic force microscopy) was used to investigate the EG surface morphology with and the morphology is similar to that observed by others [1, 12, 19]. Raman measurements were carried out on EG on both carbon (C) and silicon (Si) faces. Micro-Raman spectroscopy using a 632 nm laser shows the G peak (~1590 cm^{-1}), D peak (~1350 cm^{-1}) and 2D peak (~2700 cm^{-1}) characteristic of EG [21]. The ratio of intensities of the D-peak to G-peak, I_D/I_G ≤0.2 demonstrates the high quality of our graphene [21]. X-ray photoelectron spectroscopy (XPS) measurements were done to obtain the thickness [22] in monolayer's (ML) on EG. The thickness extracted by XPS was consistent with our FTIR measurements [12].

Fourier transform infrared reflection (FTIR) measurements (2.5 μm to 25 μm wavelength) were carried out with a blank SiC substrate, cut from the same wafer as the grown samples, as the reference (shown in Fig. 1(c). So we find differential reflectance of EG with respect to SiC substrate. Our previous work indicate that this method can be applicable to find EG thickness in no of monolayers (ML's), scattering time (τ), and Fermi level (E_f). Thickness measurement using this method is consistent with XPS measurements as explained et.al. Daas [12]. In this work, FTIR measurement was carried out as the same process described above but the chamber was filled

with the required adsorbent gas (Fig. 1(c). Reference was taken with N_2 environment (known as inert gas) and corresponding IR reflection was taken in $N_2/NO_2/NH_3$ environment consequently. All reflectance measurement presented here are the differential reflectance with respect to the SiC substrate. A more detailed analysis of this data, along with our developed theory allows the extraction of the influence of interband scattering as well, which is non-negligible at IR frequencies and high surface impurity concentrations.

4. Result and Discussion

NO_2 is a strong oxidizer with electron withdrawing capability, and is expected to decrease electron carrier concentration on the EG surface [23], while the converse is true for NH_3 as it is electron donating [24]. However, our measurements are based on EG grown on C-face SiC, which is thicker (>8ML), much greater than the 1ML screening length in graphene [25]. Thus, this layer is expected to be close to electrically neutral i.e. the Fermi level is close to the Dirac point (K and K' in the Brillouin zone). Therefore, carrier concentration will increase in both the cases regardless of whether the adsorbent is electron withdrawing or electron donating.

Polar molecules [11] change EG conductivity by a) inducing carriers in the EG and b) increasing scattering i.e. decreasing mobility. Scattering (τ) includes both intra and interband scattering, responsible for inter and intra band conductivity respectively [11]. Increase or decrease of conductivity is a tradeoff between carrier concentration (Equation (5) and scattering. Thus, it is critical to investigate the role of E_F and τ in response to gas adsorption.

Fig. 2 shows the IR reflection spectra for 9, 22 and 34 ML EG in N_2, NH_3 and NO_2 environment where we find that reflectance (indicative of conductivity, with higher conductivity leading to higher reflectance) changes for different gases due to adsorption of surface impurities. Reflectivity decreases both in NO_2 and NH_3 environments compared to N_2 with NO_2 showing greater decrease than NH_3. Because, NH_3 has lower adsorption energy which allows it to both charge interacting and non-interacting configuration [26], whereas NO_2 has higher adsorption energy (0.3~0.4 eV) [27], which forces it to accept electrons in any adsorption configuration [26]. We extract ML, E_F and intra and inter band scattering time by matching experimental data with the theory (Table 1). We also used previously developed mathematical model [12] to account for impurity adsorption where we match optical conductivity [16] at high and low frequency with conductivity in the Random Phase approximation (RPA) to extract surface impurity concentration, n_i by

$$\sigma_{T=0}^{RPA} = \frac{e^2}{\pi h}\left[\frac{n_s}{n_i G[4r_s/(2-\pi r_s)]} + \frac{n_i F[4r_s/(2-\pi r_s)]}{4n_s}\right], \quad (12)$$

where h is the Planck's constant, n_s is the surface carrier concentration, r_s, G and F function are defined as below.

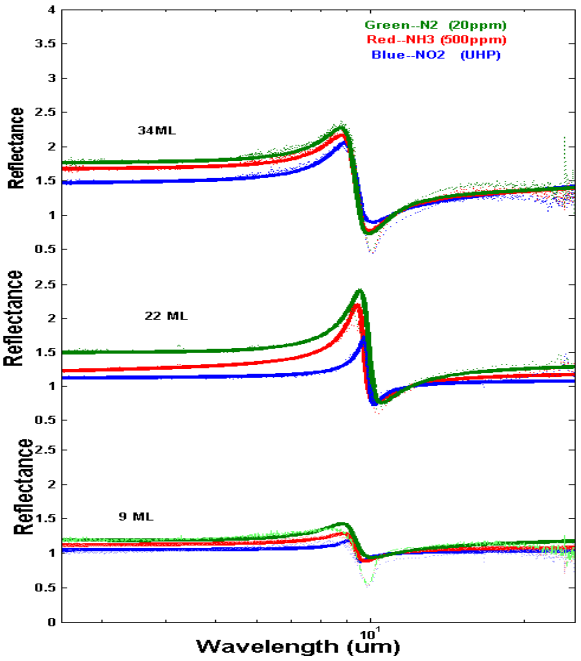

Fig. 2. (color online): Shows the IR reflection measurement while experimental data fits with the mathematical model. Extracted parameters are indicated in Table 1.

Table 1. Shows extracted parameter while experiment matches with theory.

No of Layer	Gas	Fermi level (meV)	Impurity (cm^{-2})	Intra band scattering time (s)	Inter band scattering time (s)
34	N_2	25 ± 2	$(2 \pm 0.5) \times 10^{11}$	$(2.8 \pm 0.9) \times 10^{-13}$	$(4.3 \pm 2.7) \times 10^{-14}$
	NH_3	30 ± 2	$(6 \pm 1) \times 10^{12}$	$(7.5 \pm 2) \times 10^{-15}$	$(2 \pm 1) \times 10^{-15}$
	NO_2	35 ± 2	$(2 \pm 0.6) \times 10^{13}$	$(1.4 \pm 1) \times 10^{-15}$	$(3.5 \pm 2) \times 10^{-16}$
22	N_2	45 ± 2	$(3 \pm 0.5) \times 10^{11}$	$(1.5 \pm 0.3) \times 10^{-14}$	$(2.3 \pm 0.1) \times 10^{-14}$
	NH_3	65 ± 2.5	$(7.5 \pm 1) \times 10^{12}$	$(6 \pm 3) \times 10^{-15}$	$(1 \pm 0.01) \times 10^{-15}$
	NO_2	95 ± 3	$(6 \pm 1) \times 10^{13}$	$(9 \pm 0.3) \times 10^{-16}$	$(2 \pm 0.7) \times 10^{-16}$
9	N_2	70 ± 4	$(5.1 \pm 0.5) \times 10^{11}$	$(1.5 \pm 0.1) \times 10^{-13}$	$(2.2 \pm 0.4) \times 10^{-14}$
	NH_3	90 ± 4	$(5.5 \pm 1) \times 10^{13}$	$(9 \pm 1) \times 10^{-16}$	$(3.6 \pm 1) \times 10^{-16}$
	NO_2	120 ± 4	$(1.5 \pm 0.8) \times 10^{14}$	$(4 \pm 1) \times 10^{-16}$	$(2 \pm 1) \times 10^{-16}$

$$r_s = \frac{e^2}{4\pi\varepsilon_0\varepsilon_{SiC}v_F\hbar}, \quad (13)$$

where e is the electron charge 1.6×10^{-19}C, v_F is the Fermi velocity 1.1×10^6 m/s, ε_{SiC} is the dielectric constant of SiC, which has different values for high frequency (ε_{SiC} ~6.5) and low frequency (ε_{SiC} ~9.52) regime and G and F function defined [16] as,

$$G(x) = \frac{x^2}{8}\int_0^{2\pi}\frac{\sin^2\theta}{(\sin\frac{\theta}{2}+x)^2}d\theta$$
$$\text{and} \quad (14)$$
$$F(x) = \frac{x^2}{8}\int_0^{2\pi}\frac{(1-\cos\theta)^2}{(\sin\frac{\theta}{2}+x)^2}d\theta$$

Considering two limiting values of SiC dielectric constant (high frequency~6.5 and low frequency~9.52), two different values of r_s (high frequency~0.31 and low frequency~0.21) were calculated [18]. For the high frequency r_s =0.31 was used for the conductivity

$$\sigma_{T=0}^{RPA}[highfrequency] = \frac{e^2}{\pi h}[\frac{n_s}{n_i G[4r_s/(2-\pi r_s)]}] \quad (15)$$

matching with the optical conductivity to extract impurity concentration, n_i. A similar procedure was used for the low frequency side where r_s ~0.21 arises from ε_{SiC} ~9.52 while considering

$$\sigma_{T=0}^{RPA}[lowfrequency] = \frac{e^2}{\pi h}[\frac{n_i F[4r_s/(2-\pi r_s)]}{4n_s}] \quad (16)$$

n_i extracted at both these frequency regimes was consistent. For further confirmation, we calculate intra and inter band scattering from n_i using equations presented elsewhere [16] and was found to be consistent with our extracted data within the experimental error limit.

Table 1 show the extracted carrier transport parameters for 34, 22 and 9ML samples in gaseous medium while experiment matches with theory. E_f and τ was extracted as a fitting parameter while n_i was extracted by conductivity matching both high and low frequency regime (discussed above). With N_2 gas, 34ML samples shows Fermi level of ~25 meV, close to neutral because our EG is thick. Similarly 22 and 9ML samples shows increase in Fermi level to 45 meV and 70 meV respectively because of thinner layer compared to 34ML, comparable to EG screening length ~1ML. As N_2 is an inert gas and should not contribute any impurity on the EG surface. Our extracted parameters indicate a surface impurity concentration due to N_2 gas is of $2\sim5\times10^{11}$cm^{-2}, fairly consistent with an ex-situ sample that has not had any degassing or other processing performed on it.

For NH_3 and NO_2, the surface impurity concentration is higher than N_2 because of the nature of the gas interaction (electron donating and withdrawing ability) with the carriers on the EG surface (Fig. 3). Increase in Fermi level position compared to N_2 in both the cases indicates more surface impurity concentration due to gas adsorption. For 34ML sample, change is Fermi level is very small (~5 meV in NH_3 and 10 meV in NO_2) indicates that thicker EG layer behaves more like neutral layer because of EG screening length is only ~1 ML. For 22 and 9 ML sample E_f changes are noticeably greater indicates the sensitivity of EG as presented by other researchers [16]. This thickness dependent trend clearly supports the single molecule sensitivity of single layer graphene described elsewhere [4]. E_f changes are greater in NO_2 compared to NH_3 attributes more charge transfer by NO_2 compared to NH_3. Changes of E_f is also supported by other potentiometric measurements Qazi, *et al.,* [28] where surface work function (SWF) changes are directly measured and Fermi level change was extracted from there.

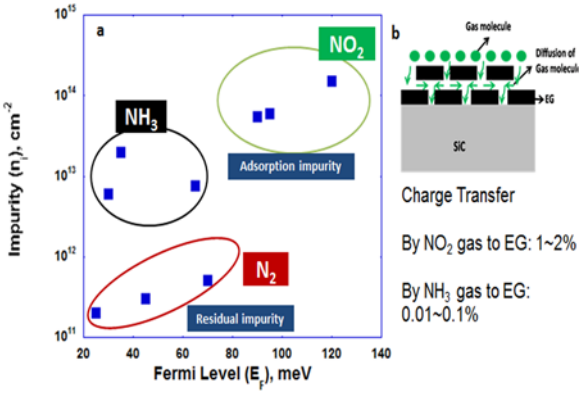

Fig. 3. (color online) (a) Impurity concentration on EG layer due to molecular adsorption. It shows that NO_2 has the charge transfer ratio of 1-2 % whereas NH_3 has only 0.01-0.1 %; (b) shows the animation of molecular adsorption through EG defect position.

We also extract scattering time (τ) through our model as theory fits with the experiments. Table 1 indicates that, both τ_{intra} and τ_{inter} shortens, due to more scattering from the adsorbed impurity. As overall conductivity is the tradeoff between carrier concentration (indication of E_f changes) and scattering (both intra, τ_{intra} and interband, τ_{inter}), So despite of the method developed by Nomani, *et al.*, [29], our method signifies the complete picture of conductivity changes with a good agreement as presented by other publications [30].

Overall conductivity decreases both for NH_3 and NO_2 compared to N_2 environment. With NO_2, overall conductivity decreases more than NH_3 despite a strong

increase in carrier concentration (Fig. 3), indicating that the EG surface has greater affinity for NO_2 adsorption, leading to much greater carrier scattering at the adsorption surface. This observation is also supported by percentage gas molecule contributing to EG surface conductivity changes. Our result indicate that NH_3 contribute 0.01~0.1 % while NO_2 contribute 1~2 % for EG surface conductivity change. This observation is consistent with other amperometric measurement [29]. However, the novelty of this work is to separate out the scattering effect which coincides with the adsorption and gives the clear picture of conductivity change.

Electronic transport in graphene is dominated primarily by two scattering mechanisms: 1) Short-range scattering, and 2) Long-range coulomb scattering [31]. Short range scattering originates from short-range factors such as lattice defects and electron-electron interactions. Short range scattering potential give rise to a scattering time that varies as 1/E and independent of temperature. Long range scattering, on the other hand, originates from the screening of charged impurities on the surface of graphene. Fig. 4 shows both intra and interband scattering varies linearly with the impurity, attributes most likely to be long range scattering dominated.

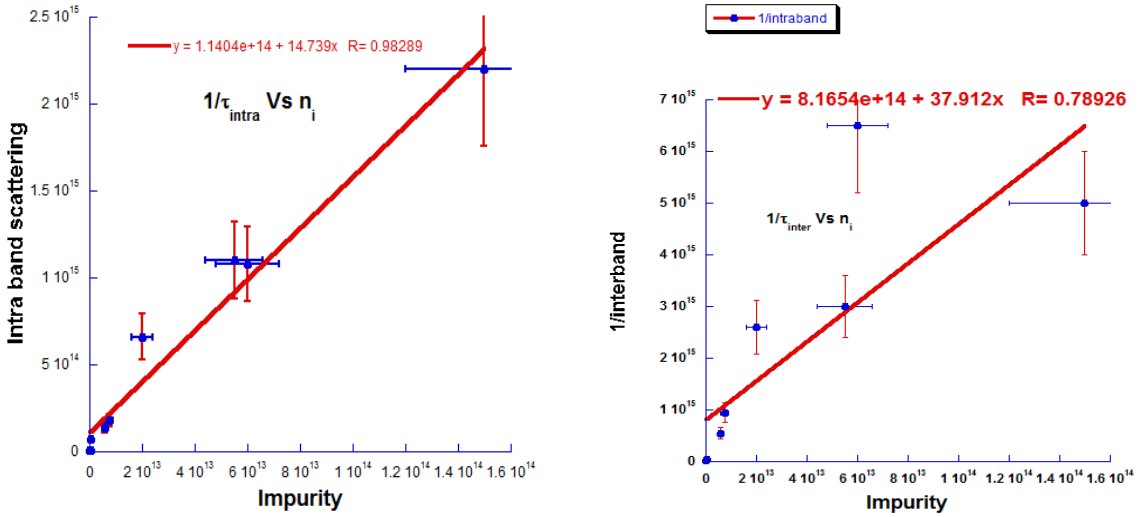

Fig. 4. Scattering time as a function of impurity concentration.

Charge impurity scattering [32], For screened coulomb scattering that leads to a conductance which is proportional to $\sqrt{n_s}$. So, linear relation between conductance and $n_s$$n_S$is the evidence of presence of charged impurity scattering. Our previous works [12] shows no significant contribution of intraband scattering because of no gas adsorbent molecule presence. With the adsorbent gas molecule n/ni significantly increases because of percentage charge transfer through the EG layer, supported by amperometric measurement, increases the charge impurity scattering, as a result interband scattering plays a dominant role which cannot be neglected even at DC.

5. Conclusion

In summary, we find that the infrared carrier transport in EG can be described only by accounting for the influence of interband scattering. In doing so, we find a self-consistent explanation of carrier transport in EG, where carrier scattering (interband and intraband) increases in response to surface impurities, along with a change in carrier concentration caused by charge transfer between the molecules and EG. This result was verified by an amperometric measurement also. This leads to an increase/decrease in overall conductivity/reflectivity depending on the tradeoff between scattering and carrier concentration. The most significant part of this study is that it gives us both carrier density and scattering (both intra and interband) considering the percentage charge transfer through the EG layer, attributes the doping concentration as well as overall conductivity change on EG films. This study is significantly important for EG sensing behavior as well as EG based FET devices.

Acknowledgement

The authors would like to acknowledge the Southeastern Center for Electrical Engineering Education, and the National Science Foundation (NSF) ECCS-EPDT Grant #1029346 under the supervision of program director Rajinder Khosla for funding this work.

References

[1]. A. K. Geim, K. S. Novoselov, The Rise of Graphene, *Nature Materials*, Vol. 6, 2007, pp. 183-191.

[2]. Lei Gong, Ian A. Kinloch, Robert J. Young, Ibtsam Riaz, Rashid Jalil, Konstantin S. Novoselov, Interfacial Stress Transfer in a Graphene Monolayer Nanocomposite, *Advanced Materials*, Vol. 22, No. 24, 2010, pp. 2694-2697.

[3]. Alexander A. Balandin, Suchismita Ghosh, Wenzhong Bao, Irene Calizo, Desalegne Teweldebrhan, Feng Miao, Chun Ning Lau, Superior thermal conductivity of single-layer graphene, *Nano Lett.*, Vol. 8, No. 3, 2008, pp. 902-907.

[4]. Biplob K. Daas, W. K. Nomani, Kevin M. Daniels, Tangali S. Sudarshan, Goutam Koley, M. V. S. Chandrashekhar, Molecular Gas Adsorption Induced Carrier Transport Studies of Epitaxial Graphene using IR Reflection Spectroscopy *Materials Science Forum*, Vol. 717-720, 2012, pp. 665-668.

[5]. J.-H. Chen, C. Jang, S. Adam, M. S. Fuhrer, E. D. Williams, M. Ishigami, Charged-impurity scattering in graphene, *Nature Physics*, Vol. 4, No. 5, 2008, pp. 377-381.

[6]. A. Bostwick, T. Ohta, T. Seyller, K. Horn, E. Rotenberg, Quasiparticle Dynamics in Graphene, *Nature Physics*, Vol. 3, No. 1, 2007, pp. 36-40.

[7]. Niraj Sinha, Jiazhi Ma, John T. W. Yeow, Carbon Nanotube-Based Sensors, *J. of Nanoscience and Nanotechnology,* Vol. 6, No. 3, 2006, pp. 573–590.

[8]. B. K. Daas, M. M. Islam, Iftekhar A. Chowdhury, Feng Zhao, T. S. Sudarshan, M. V. S. Chandrashekhar, Doping Dependence of Thermal Oxidation on n-Type 4H-SiC, *IEEE Transactions on Electron Devices,* Vol. 58, No. 1, 2011, pp. 115-121.

[9]. Shamaita S. Shetu, B. Daas, K. M. Daniels, T. S. Sudarshan, G. Koley, M. V. S. Chandrashekhar, Selective multimodal gas sensing in epitaxial graphene by Fourier transform infrared spectroscopy, *IEEE Sensors*, 2013, pp. 1-3.

[10]. Y. Dan, Y. Lu, N. J. Kybert, Z. Luo, A. T. C. Johnson, Intrinsic response of graphene vapor sensors, *Nano Lett*., Vol. 9, No. 4, 2009, pp. 1472-1475.

[11]. B. K. Daas, W. K. Nomani, K. M. Daniels, T. S. Sudarshan, Goutam Koley, A. Mendez Torres, M. V. S. Chandrashekhar, Advance in Molecular Gas Sensing Studies Using Epitaxial Graphene, *Transactions of the American Nuclear Society*, Vol. 105, 2011, pp. 260-261.

[12]. B. K. Daas, K. M. Daniels, T. S. Sudarshan, M. V. S. Chandrashekhar, Polariton enhanced infrared reflection of epitaxial grapheme, *J. Appl. Phys*., Vol. 110, No. 11, 2011, pp. 113114-1 - 113114-6.

[13]. V. P. Gusynin, S. G. Sharapov, J. P. Carbotte, Unusual microwave response of dirac quasiparticles in grapheme, *Phy. Rev. Lett.*, Vol. 96, No. 25, 2006, 256802.

[14]. B. K. Daas, Amit Dutta, Electromagnetic dispersion of surface plasmon polariton at the EG/SiC interface, *Journal of Material Research*, Vol. 29, Issue 21, 2014, pp. 2485-2490.

[15]. T. Stauber, N. M. R. Peres, A. K. Geim, Optical conductivity of graphene in the visible region of the spectrum, *Phy. Rev. B*, Vol. 78, No. 8, 2008, 085432.

[16]. S. Y. Liu, X. L. Lei, Norman J. M. Horing, Diffusive transport in graphene: The role of interband correlation, *J. Appl. Phys*., Vol. 104, No. 4, 2008, pp. 043705-1 - 043705-6.

[17]. Kai Fai Mak, Mathew Y. Sfeir, Chun Hung Lui et al Optical conductivity of graphene, *Phy. Rev. Letter*, Vol. 101, No. 196405, 2008.

[18]. Dmitriy Korobkin, Yaroslav Urzhumov, Gennady Shvets, Enhanced near-field resolution in midinfrared using metamaterials, *J. Opt. Soc. Am. B*, Vol. 23, No. 3, 2006, pp. 468-478.

[19]. C. Berger, *et al*., Ultrathin epitaxial graphite: 2D electron gas properties and a route toward graphene-based nanoelectronics, *J. Phys. Chem. B*, Vol. 108, 2004, pp. 19912-19916.

[20]. Kevin M. Daniels, B. K. Daas, N. Srivastava, C. Williams, R. M. Feenstra, T. S. Sudarshan, M. V. S. Chandrashekhar, Evidences of electrochemical graphene functionalization and substrate dependence by Raman and scanning tunneling spectroscopies, *J. Appl. Phys.,* Vol. 111, 2012, 114306.

[21]. Ferrari A. C., *et al*., Raman Spectrum of Graphene and Graphene Layers, *Phys. Rev. Lett*., Vol. 97, No. 18, 2006.

[22]. P. J. Cumpson, The Thickogram: a method for easy film thickness measurement in XPS, *Surface and Interface Analysis*, Vol. 29, No. 6, 2000, pp. 403-406,

[23]. J. Kong, N. R. Franklin, C. Zhou, M. G. Chapline, S. Peng, K. Cho, H. Dai, Nanotube molecular wires as chemical sensors, *Science*, Vol. 287, No. 5453, 2000, pp. 622-625.

[24]. Sergey Novikov, Alexandre Satrapinski, Natalia Lebedeva, Ilkka Iisakka, Sensitivity Optimization of Epitaxial Graphene-Based Gas Sensors, *IEEE Transaction on Instrumentation and Measurement*, Vol. 62, No. 6, June 2013, pp. 1859-1864.

[25]. Taisuke Ohta, Aaron Bostwick, J. L. McChesney, Thomas Seyller, Karsten Horn, Eli Rotenberg, Interlayer Interaction and Electronic Screening in Multilayer Graphene Investigated with Angle-Resolved Photoemission Spectroscopy, *Phys. Rev. Lett.*, Vol. 98, No. 20, 2007, 206802.

[26]. I. Iezhokin, P. Offermans, S. H. Brongersma, A. J. M. Giesbers, High sensitive quasi freestanding epitaxial graphene gas sensor on 6H-SiC, *Applied Physics Letters*, Vol. 103, No. 5, 2013, pp. 053514-1 - 053514-5.

[27]. T. O. Wehling, K. S. Novoselov, S. V. Morozov, E. E. Vodvin, M. I. Katsnelson, A. K. Geim, A. I. Lichtenstein, Molecular Doping of Graphene, *Nano. Lett*, Vol. 8, No. 1, 2008, pp. 173-177.

[28]. Biplab Sanyal, *et al.*, Molecular adsorption in graphene with divacancy defects, *Phys. Rev. B*, Vol. 79, No. 11, 2009, 113409.

[29]. Biplob Kumar Daas, Plasmonics using high quality epitaxial graphene: an approach towards next-generation optical computing, PhD Dissertation, *University of South Carolina,* 2012.

[30]. O. Leenaerts, B. Partoens, F. M. Peeters, Adsorption of H_2O, NH_3, CO, NO_2, and NO on graphene: A first-principles study, *Phys. Rev. B*, Vol. 77, No. 12, 2008, pp. 125416-125422.

[31]. S. Adam, E. H. Hwang, S. Das Sarma, Scattering mechanisms and Boltzmann transport in graphene, *Physica E*, Vol. 40, No. 5, 2008, pp. 1022-1025.

[32]. E. H. Hwang, S. Adam, S. Das Sarma, Carrier Transport in Two-Dimensional Graphene Layers, *Phy. Rev. Lett.*, Vol. 98, No. 18, 2007, 106806.